

# Chapter 7

## Systematic Errors

*The results obtained in the previous chapter depend on many assumptions about our knowledge of the relevant physics backgrounds, detector performance, and (crucially so) on the accuracy of the Monte Carlo simulation. In this chapter, we explore the sensitivity of our results to errors in the assumptions used both in the simulation and when analyzing the real data. In many cases, we can directly measure this sensitivity by modifying some feature of the simulation and then repeating the entire analysis; any shift in the results is interpreted as the scale of the uncertainty associated with the selected feature of the simulation. Because the neutrino reconstruction technique relies on the reconstruction of the entire event, the list of potential sources of systematic error turns out to be quite lengthy. We find that the total systematic uncertainty is significantly smaller than the statistical errors, and conclude that our findings as presented in the last chapter are robust, particularly insensitive to the details of the  $b \rightarrow c \ell \nu$  and  $b \rightarrow u \ell \nu$  modeling.*

### 7.1 Overview

This analysis relies heavily on the Monte Carlo simulation of both the  $b \rightarrow u \ell \nu$  signal and the  $b \rightarrow c \ell \nu$  background. Our knowledge of the true physics of these decays and the detector signatures they generate is limited, however, and prompts us to consider the sensitivity of our results to the myriad assumptions that have gone into constructing the simulation and, subsequently, in developing the analysis. The quantification of these systematic errors is an important part of the analysis effort, in essence an assessment of the “risk” that our results are “wrong,” or, alternatively, a measurement of the degree to which the results reflect real features of the data and are not contingent upon artificial or happenchance features of the simulation.

We divide the sources of systematic error into two categories: detector simulation and model dependence. The Monte Carlo simulation of the CLEO detector has been calibrated to reproduce distributions observed in data as broadly as possible, but there are still aspects of the simulation subject to lingering uncertainties, *e.g.* the deposition of energy in the crystals by neutral hadrons. Particularly because our analysis technique utilizes features of the entire event to estimate the kinematics of the missing neutrino, the faithful simulation of detector response across the full spectrum of particle momenta and energies is vital. Derived quantities such as particle identification variables, event net charge, and shower shape variables all rely on the accuracy of the lower-level detector simulation, and the

consequences of inaccuracies in the simulation of each of these aspects must be addressed. In most cases, we can modify features of the existing simulated samples, varying their properties in a manner consistent with our confidence in the underlying detector simulation, and then measure directly the attendant shift in the results by re-analyzing the altered samples. Such studies are characterized as “knob turns” since some feature of the detector simulation is “dialed” away from its default value, and the impact of the change is determined simply by re-applying the standard analysis technology.

Our limited knowledge of generic  $B$  decay and the lack of a complete understanding of inclusive  $b \rightarrow u \ell \nu$  decay induces similar uncertainties, broadly described as the “model dependence” of the analysis. The emphasis in this category is on the uncertainties in our physics-level description of the decays, and is typically harder to assess. We use a combination of knob-turn and re-weighting techniques to quantify them.

## 7.2 Detector Simulation

From an armchair perspective, we can identify several different categories of “mistakes” in the detector simulation that could lead to inaccuracies sufficient to jeopardize confidence in our results: parametric mistakes, such as the use of incorrect drift functions in the drift chamber simulation; physics mistakes, such as neglecting a particular type of material interaction; and implementation mistakes, such as code or logic bugs. In addition to these possibilities, the inputs to the simulation itself may be faulty, *e.g.* in the description of the amount, location, and type of material in the detector. Particles scatter and lose energy when traveling through matter, and small inaccuracies in the material description can significantly alter particle reconstruction efficiencies through pre-showering and premature stopping.<sup>1</sup>

Assessing the sensitivity of our measurement to the thousands of details of the full simulation package is practically impossible if we try to consider each component of the simulation individually. Turning each available “knob” or parameter in the simulation and then re-generating the  $\sim 40$  M simulated events we use in the analysis is simply not feasible. There is often no well-defined scale for such knob turns, and many of them are so far removed from actual reconstruction-level quantities that is hard to even qualitatively understand the possible impact on analysis variables. Lastly, re-generating all of our simulated data, for each potential knob,

---

<sup>1</sup>In the past, for instance, a discrepancy in  $\pi^0$ -finding between data and Monte Carlo was traced, in part, to a mistake in the description of the material in the time-of-flight counters immediately in front of the crystals [90]. An incorrect radiation length caused the photons from simulated  $\pi^0 \rightarrow \gamma\gamma$  decays to lose too much energy before showering in the cesium iodide crystals.

would require near infinite time, CPU, and storage resources.

Instead, we consider the impact of simulation mistakes on our results by deliberately altering those event characteristics that are directly or implicitly employed in the analysis. While recognizing that inaccuracies in the simulation might arise from mistakes like those described above, we leave open the possibility of other underlying sources of error, and simply absorb all such sources into a small number of effective knobs that capture the true simulation effects to which we're more sensitive. The other advantage of this small set of tangible, reconstruction-level features is that, because of their practical nature, it is much easier to assess the accuracy of their simulation with independent data-Monte Carlo comparison studies.

The systematic uncertainties associated with the detector simulation that we consider are:

- Splitoff modeling
- $K_L$  energy deposition
- Shower-finding efficiency
- Shower resolution
- Splitoff rejection
- Track-finding efficiency
- Tracking resolution
- Particle ID resolution

These issues are generally addressed with knob-turning studies. Note that the central question in each case is how well the Monte Carlo simulation matches the corresponding quantity in data. That is, for instance, the absolute shower efficiency itself is not in question—the issue is whether the shower-finding efficiency in Monte Carlo matches that in data, regardless of whatever the actual inefficiency might be.

In most cases, the data-Monte Carlo discrepancies can be of either sign; for instance, the shower energy resolution in the simulation might be better or worse than that in data. For those cases where it is not possible to turn the knob associated with a particular systematic in both directions, we settle for measuring the effect of a one-sided knob turn and then assume that a similar deviation applies for an excursion in the other direction. In a few cases, we “over-turn” the knob to

enhance the magnitude of the effect and then scale back the measured shift in the results, assuming that the response is, in fact, linear.<sup>2</sup>

We turn each knob individually, ultimately assuming that the sources of systematic error will combine incoherently.

We discuss the assessment of each of these uncertainties in more detail in the following sections. The numerical results of the knob turns will be presented in summary form somewhat later.

## 7.2.1 Shower Reconstruction

Calorimetry is an important part of neutrino reconstruction, and we consider several aspects of the simulation of energy deposition and shower reconstruction.

### Splitoff modeling (*AddShowers* knob)

We consider the impact of a possible discrepancy between data and Monte Carlo in the number of splitoff showers per hadron. While average shower and track multiplicity in  $B\bar{B}$  events is known to be reasonably well-modeled, there is some uncertainty about the accurate simulation of the number of excess unmatched or splitoff showers per hadron. This may be due to actual inaccuracies in the modeling of splitoff shower production or a mistake in the material description which could cause particles to pre-shower earlier in the detector (or simply more often in data than in Monte Carlo), and so alter the average shower multiplicity.

To assess the importance of such a data-MC difference for our analysis, we artificially insert additional showers into simulated events, using an energy spectrum for splitoff showers measured previously [112]. The rate at which we add the extra showers is 0.029 showers per charged hadron, a scale determined by a past study that counted showers in clean  $\gamma\gamma \rightarrow K_S K_S$  events [113].

### $K_L$ energy deposition (*BoostKlongShowers* knob)

We address the possibility of mis-modeling of  $K_L$  showers by increasing the energy of calorimeter showers matched to  $K_L$ 's by 20%, allowing for a significant under-estimate of the true energy deposition. This figure is chosen based on previous CLEO studies of the energy deposited by  $K^+$  in the crystals [115], and from a more recent comparison of data and Monte Carlo modeling of  $K_L$

---

<sup>2</sup>There has been some debate about whether cranking a knob farther than necessary is actually wise, especially since assumptions of linearity seem slightly suspect for complex simulations. However, following ample historical precedent, we adopt the same method.

and  $K^0$  showers reconstructed through the decay chain  $e^+e^- \rightarrow \gamma\phi$ , with  $\phi \rightarrow K_S K_L, K^+ K^-$  [116].

### Shower-finding efficiency (*DropShowers* knob)

Material discrepancies or errors in the simulation of lateral shower profiles can lead to data-MC differences in the number of showers found in an event. We randomly discard 3% of showers matched to photons to explore such effects. Past CLEO studies have concluded that the data-MC difference in the shower efficiency is 2%, so we scale back the exaggerated effect of this knob by 2/3.

### Shower resolution (*SmearPhotonShowers* knob)

We consider the effects of mistakes in the modeling of shower energy resolution: for showers matched to photons, we smear the reconstructed energy 10% further from the true photon energy,

$$E_{\text{shwr}} \rightarrow E_{\text{shwr}} + 0.10(E_{\text{shwr}} - E_\gamma). \quad (7.1)$$

### Splitoff rejection (*SmearSplitoff* knob)

The Splitoff neural net rejection package was trained on a combination of real and simulated data. We assess the systematic error inherent in its decision-making algorithms by effectively “de-tuning” the neural net. We insert a noise or smearing term in the net output  $NN$  according to

$$NN \rightarrow NN \pm s |G| |NN \pm 1|. \quad (7.2)$$

Here  $G \sim N(0, 1)$  is a unit-normal Gaussian random variable and  $s = 0.2$  sets the scale of the smearing. Smearing in the “+” direction is applied for showers that are tagged to photons, and in the “−” direction for all others. Neural net responses close to  $NN = +1$  identify splitoff showers, and  $NN = -1$ , real photons, so the effect of the smearing is to bias true photons in the splitoff direction, and all other showers in the photon-like direction. The performance of the neural net is thus impaired in a systematic fashion. See Appendix B for more discussion of the implementation of the neural net and the incorporation of smearing.

Fig 7.1 demonstrates the effect of this smearing on the neural net’s response for a sample of non-isolated unmatched showers. The modified net output is systematically biased toward the photon end of the spectrum for showers not tagged to photons, and promoted toward the splitoff end for those that are matched to photons.

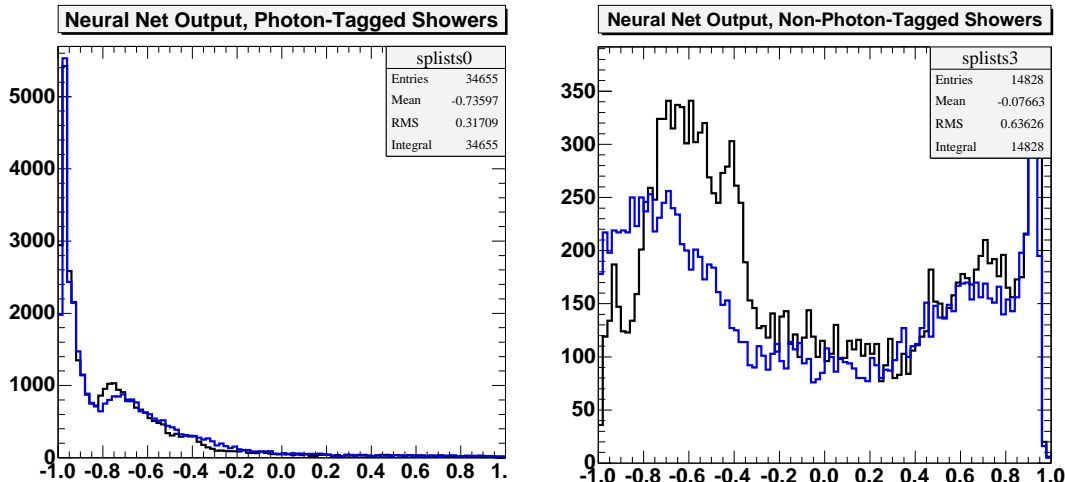


**Figure 7.1:** Smearing of Splitoff neural net output, for a sample of non-isolated showers in Monte Carlo. The plot on the left is for showers matched to photons, and that on the right, for showers not so matched. The distribution of the neural net output before smearing is shown in black; after setting the *SmearSplitoff* knob to 0.2, the distributions are systematically altered to those shown in blue. Photons are shifted toward the splitoff direction, and non-photons in the photon direction.

## 7.2.2 Track Reconstruction

The foundation of neutrino reconstruction is excellent track reconstruction, at the track-finding stage and in the subsequent resolution on the momentum of the tracks that are found.

Previous studies have already demonstrated that there is little systematic difference in the performance of the Trkman package between data and Monte Carlo by comparing, for instance, net charge distributions. Hence we do not evaluate an additional systematic for our use of Trkman.

### Track-finding efficiency (*DropTracks* knob)

We also assess the importance of a systematic difference between track-finding efficiency in data and Monte Carlo. Any such difference is more likely the result of mistakes in material description than a difference in the performance of pattern recognition and actual track reconstruction in data and Monte Carlo. Too little material in the Monte Carlo can decrease the average number of inelastic hadronic interactions particles undergo as they traverse the detector and encounter detector material. The result is that more particles in the simulation than in data will survive the flight across the full volume of the tracking chambers, effectively inflating

the track-finding efficiency. Discrepancies can also arise from the simulation of drift chamber hit efficiency (the likelihood that a cell through which a track has passed will register a hit) or from the charge division calibration used in the VD to reconstruct  $z$  information for tracks.

In close analogy to the evaluation of the shower efficiency systematic, we randomly drop reconstructed tracks from the event before the analysis machinery is set in motion. Independent investigations have combined track-embedding studies with extensive Monte Carlo knob-turning to assess a momentum-dependent track-finding efficiency systematic across the full spectrum of track momentum [95]. Using these figures as a guide, we eliminate high- and low-momentum tracks at different rates, given by:

$$f_{drop} = \begin{cases} 2.6\% & |p| < 250 \text{ MeV} \\ 0.75\% & |p| \geq 250 \text{ MeV} \end{cases} . \quad (7.3)$$

### Tracking resolution (*SmearTracks* knob)

We assess the impact of a systematic difference in track momentum resolution by smearing reconstructed values further from the “truth,” much as for the *SmearPhotonShowers* knob. Here, the prescription is once again a 10% smearing according to:

$$\vec{p}_{\text{trk}} \rightarrow \vec{p}_{\text{trk}} + 0.10(\vec{p}_{\text{trk}} - \vec{p}_{\text{true}}). \quad (7.4)$$

### 7.2.3 Particle ID

We explore our sensitivity to hadron identification differences between data and Monte Carlo by systematically (but separately) degrading the time-of-flight and  $dE/dx$  information used in the particle identification algorithm. The TOF significance variables  $\chi_h^{\text{TOF}}$  are each increased by 0.5, corresponding to a systematic mistake in the simulation of the TOF response for all hypotheses. We shift the  $dE/dx$  significance variable up (down) by 0.25 for tracks with momentum below (above) 1.2 GeV. This momentum marks the cross-over point in  $dE/dx$  separation between pions and kaons. Measurements in Monte Carlo reveal that these shifts increase the number of PID mistakes per event by slightly less than 5%.

As points of comparison, we also run the analysis machinery in PID-blind and PID-perfect modes, where all particles are either labeled as pions or according to generator-level truth, respectively.<sup>3</sup> These two variations essentially bracket the spectrum of possible PID systematics. We confirm a measurable shift in the analysis central values when they are applied, roughly comparable to the shifts

---

<sup>3</sup>Identified leptons are not modified in these variations, consistent with the special, data-based simulation of lepton efficiency.

observed for the individual *Degrade* knobs. Using these extremes to assess the PID systematic directly is difficult, however, since there is no natural guide for comparing these changes to the actual level of confidence we have in our PID algorithms. Instead, we use these two variations simply as consistency checks; they serve to increase our confidence in the more judicious PID degradation described previously.

## 7.2.4 Summary of Detector Systematics

Each knob turn results in thirty new sets of fit results. Rather than tabulating these explicitly, we display them graphically in Fig 7.2. Since the errors on the impact ratios  $R_a$  are largely determined by the underlying WA yield, we show the preliminary results of the detector knob-turning studies as parametric plots of the shift in the WA yield, plotted against the average hadronic mass of each WA sample, *i.e.* in the same manner as used to display the central values in Ch 6.

The knob-turning studies were initiated slightly before the final selection of the conditions (*e.g.* final event weights) for the nominal fit, so the appropriate reference point for the knob-turns is not the nominal fit described in Ch 6. Instead, a suitable *KnobReference* sample is prepared and the fractional changes from these results are then transferred to the final *Nominal* results.

## 7.3 Physics Simulation

We review the components of our simulation at the “physics level” to evaluate how sensitive our results are to assumptions about the composition and shapes of various backgrounds. For a neutrino reconstruction analysis, a chief concern is the accuracy of the number and nature of the missing particles in an event, particularly  $K_L$ ’s and additional neutrinos. We also consider variations of the modeling of the  $b \rightarrow c \ell \nu$  background and the  $b \rightarrow u \ell \nu$  signal. Because the WA signal is reasonably well separated from the bulk of the  $b \rightarrow c \ell \nu$  rate, we expect the dependence on the modeling of this background to be rather small.

We again discuss the evaluation of these sources of systematic error before presenting the results of these studies.

### 7.3.1 Generic $B$ Decay

Resolution on the kinematics of the undetected neutrino is dominated by the presence of undetected neutrals in the event that are produced in the generic decay of the other  $B$  in the event; as we’ve seen, these particles are primarily  $K_L$ ’s

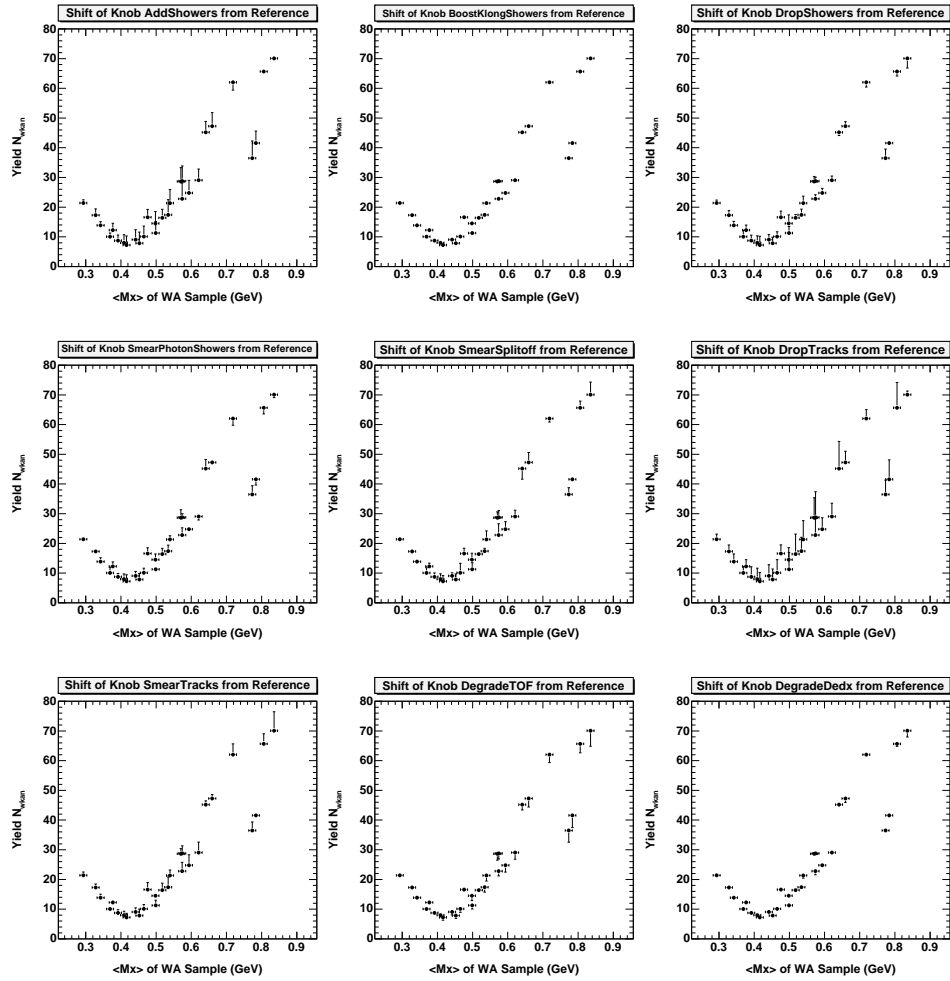


**Figure 7.2:** Systematic shift in WA yields for each detector simulation knob. The central values from the nominal simulation are shown as points, and the “error bars” indicate the (one-sided) shift in the fit results when the specified knob is “turned.” From left to right, top to bottom, the knobs shown are: *AddShowers*, *BoostKlongShowers*, *DropShowers*; *SmearPhotonShowers*, *SmearSplitoff*, *DropTracks*; *SmearTracks*, *DegradeTOF*, *DegradeDedx*. Statistical errors are not drawn.

and second neutrinos. Our default Monte Carlo samples already incorporate re-weightings intended to bring the simulated data into agreement with the real data in these regards, but there is some uncertainty on the weights that are used. The re-weighting scheme allows us to assess the impact of these residual uncertainties in a straightforward fashion. We simply alter the weight and observe the consequent shift in the analysis results, if any.

As a matter of definition, these two systematic errors are later considered part of the neutrino reconstruction systematic rather than a contribution to model-dependence.

### $K_L$ multiplicity

As described in Sec 5.9.2, we apply a re-weighting of  $(1.072)^{N_{K_L}}$  to the default Monte Carlo simulation to increase the average number of  $K_L$ 's per event to match measurements recently made in data. We take the error on the central value of that study ( $1.072 \pm 0.010$ ) as the systematic error on the re-weighting, and re-weight all of the simulated samples alternatively with a geometric weight built from 1.062 (*KlongWeightDown*) and 1.082 (*KlongWeightUp*). The results of these two knob turns, one in each direction, are shown in Fig 7.3.

When this systematic error is combined with others, we symmetrize the errors according to the conservative recipe

$$\sigma^2 = \frac{\sigma_{\text{hi}}^2 + \sigma_{\text{lo}}^2}{2}. \quad (7.5)$$

### Secondary lepton spectrum

Similarly, we include a re-weighting of the secondary lepton momentum spectrum and branching fraction in our default simulation. The systematic error on this re-weighting is assessed by varying the weight spectrum within its errors, which are determined as described in Sec 5.9.3 by accounting for the errors on the two source spectra used to construct the secondary lepton spectrum. The different weight spectra that result were shown earlier in Fig 5.27. Note we do not consider a systematic error on the branching fraction.

The shift in the analysis results when the lepton momentum spectrum is re-weighted using its high and low variations are shown in Fig 7.3. The systematic error for this source is also later symmetrized according to Eqn 7.5.

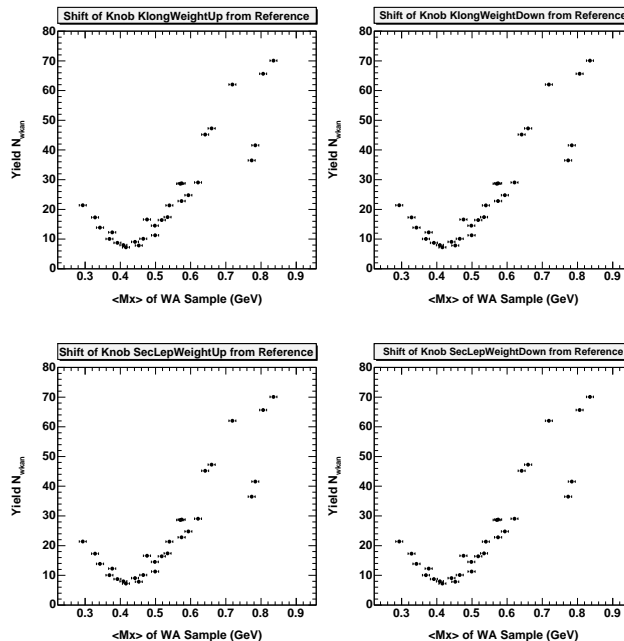


**Figure 7.3:** Systematic shift in WA yields for generic  $B$  decay simulation knobs. The central values from the nominal simulation are shown as points, and the “error bars” indicate the (one-sided) shift in the fit results when the specified knob is turned in the direction indicated. From left to right, top to bottom, the knobs shown are:  $KlongWeightUp$ ,  $KlongWeightDown$ ;  $SecLepWeightUp$ ,  $SecLepWeightDown$ . Statistical errors are not drawn.

### 7.3.2 $b \rightarrow c \ell \nu$ Modeling

We explore the sensitivity of our results to the modeling of the  $b \rightarrow c \ell \nu$  background by modifying the parameterization of the  $B \rightarrow D^* \ell \nu$  form factors. Since this mode dominates the semileptonic  $B$  decay rate, we consider these modifications as sufficient for understanding the sensitivity to the modeling of the  $b \rightarrow c \ell \nu$  background as a whole.

In particular, we modify the standard re-weighting described in Sec 5.9.4 as shown in Table 7.1.

The form factor slope  $\rho^2$  and curvature  $c$  are intimately related, and given an observed  $w$  distribution in data, one parameter cannot be modified independently of the other without impacting the overall agreement with the measured distribution. Lipeles [78] has devised a technique for addressing this problem, noting that the ratio  $\mathcal{R}_{w_1, w_2}$  of the form factor  $h_{A_1}(w)$  evaluated at two representative values of  $w$  should remain the same under re-parameterizations of the form factor. Using

**Table 7.1:**  $B \rightarrow D^* \ell \nu$  form factor variations used to assess dependence on  $b \rightarrow c \ell \nu$  modeling. Because of the intimate connection between the form factor slope  $\rho^2$  and curvature  $c$ , when one parameter is modified, the other must be updated as well to remain consistent with the underlying measurements made in data.

Variation	$\rho^2$	$c$	$R_1(1)$	$R_2(1)$	Notes
Nominal	1.20	0.35	1.24	0.72	See Sec 5.9.4
Raise $\rho^2$	1.45	0.80	1.24	0.72	Update $c$ based on new $\rho^2$
Lower $\rho^2$	0.94	0.59	1.24	0.72	Update $c$ based on new $\rho^2$
Vary $c$	0.88	0.0	1.24	0.72	Update $\rho^2$ based on new $c$
HFAG '04	0.675	1.163	1.24	0.72	Halve $c$ , update $\rho^2$

the Isgur-Wise expansion for  $h_{A_1}(w)$ , we thus require that the quantity

$$\mathcal{R}_{w_1, w_2} = \frac{h_{A_1}(w_1)}{h_{A_1}(w_2)} = \frac{1 - \rho^2(w_1 - 1) + c(w_1 - 1)^2}{1 - \rho^2(w_2 - 1) + c(w_2 - 1)^2} \quad (7.6)$$

be invariant under a new choice of  $(\rho^2, c)$ ; if one parameter is modified, the other must be updated as well. For  $B \rightarrow D^* \ell \nu$ , a reasonable choice is  $(w_1, w_2) = (1.15, 1.35)$ , bounding the region in  $w$  where the bulk of the decay rate lies. Inverting this expression as appropriate, we can compute matching values for  $c$  and  $\rho^2$  as needed when one parameter or the other is changed. We use the world-average values  $\rho^2 = 1.51$  and  $c = 1.39$  to initially evaluate  $\mathcal{R}_{w_1, w_2}$ .

The results of these variations are depicted in Fig 7.4, which shows the shift in the WA yields for each of the alternative form factor re-weightings. Noting that the spread in  $b \rightarrow c$  model dependence is firmly bracketed by the uncertainty in  $\rho^2$ , we take the high and low variations of this parameter as a measure of the systematic error for this source, but inflate the spread by another 25% to cover the possibility of additional smaller systematics not fully explored, *e.g.* variation with  $R_{1,2}$ . We present the contribution of this uncertainty to the various impact ratios  $R_a$  in Sec 7.5.

### 7.3.3 $b \rightarrow u \ell \nu$ Modeling

Much less is known with certainty about  $b \rightarrow u \ell \nu$  decays, making it harder to limit our uncertainty in a systematic fashion. However, we can explore significant variations of the default modeling within the broad framework of the InclGen simulation. Five variations of the InclGen inclusive model are used to generate fully independent event samples, as described in Sec 5.2.2. To briefly review, the `bsg(hi/lo)` samples use different values for the parameters of the inclusive shape

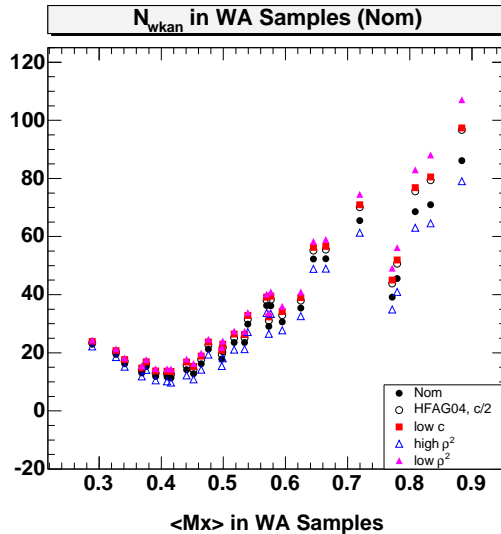


**Figure 7.4:** Effect of the  $b \rightarrow c$  model variations described in the text on the WA yields. The reference sample for these variations is designated “Nom” in the legend. Statistical errors are not drawn.

function; the alternative values are selected from the  $\pm 1\sigma$  extremes evaluated in CLEO’s recent  $b \rightarrow s\gamma$  photon energy spectrum analysis [128]. The `x0/hi/1o` samples turn off the exclusive resonances and hadronize all  $b \rightarrow u\ell\nu$  decays as non-resonant  $n$ -body systems,  $n \geq 2$ .

We repeat the analysis, thirty fits and all, for each of the five alternative  $b \rightarrow u\ell\nu$  samples. The resulting shifts in the WA yields are shown in Fig 7.5, compared to the `newbsg` reference sample. Although the `x0` samples represent more extreme variations of the basic model, the hadronic mass spectrum in these purely inclusive samples has little rate at low mass, and so prevents the  $b \rightarrow u\ell\nu$  rate from reaching as high in  $q^2$  and  $E_\ell$  as the default model and its variations.

We choose the `bsghi/1o` pair as a conservative estimate of the  $b \rightarrow u$  model dependence, and symmetrize the errors for the assignment of a  $\pm 1\sigma$  uncertainty.

## 7.4 Cross Checks

We explore the stability of our results with several consistency checks that sacrifice statistical power but allow for comparisons that would otherwise be impossible. For instance, we divide the sample into two sub-samples based on the flavor of the signal lepton,  $e$  or  $\mu$ , and fit them independently. We find results that are very consistent with the fit to the combined data sample and with each

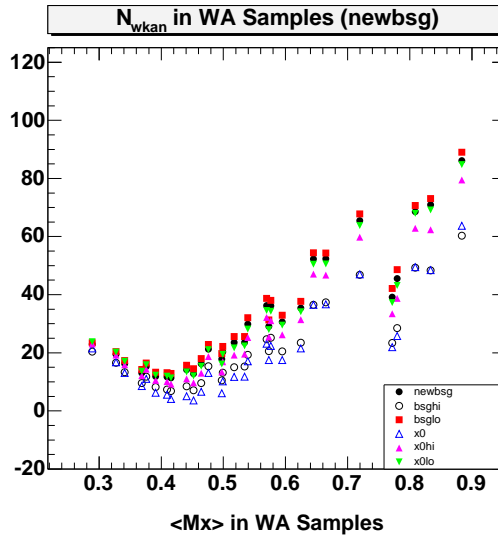


**Figure 7.5:** Effect of changes in  $b \rightarrow u$  modeling on the WA yields, as measured for the different InclGen-based samples described in the text. The reference sample for these variations is designated “newbsg” in the legend. Statistical errors are not drawn.

other.<sup>4</sup> We also separate the data according to dataset (CLEO II or II.V), and fit these two pools separately. Again, we find results that agree well (within statistical errors) with each other and that sum to a value consistent with the combined fit.

As an additional check, we try floating the continuum normalization rather than applying the fixed scaling determined from luminosity and beam-energy considerations. The fit result for this additional free parameter is within 10% of our dead-reckoned scaling, with comparable statistical errors, indicating excellent agreement. The impact on the WA yields is insignificant, as we expect since there is little continuum background at high  $q^2$  where the WA component is found.

Similarly, we perform a fit allowing the normalization of the fake lepton background to vary, and find results for the scale factor that are consistent with expectation. Again, the impact on the raw WA yields is negligible.

## 7.5 Summary of Results, with Systematic Errors

Having described the evaluation of numerous contributions to the total systematic uncertainty on our results, we summarize the results in Tables 7.2–7.4 and Figs 7.6–7.8, one of each for each impact ratio. The statistical errors dominate the

---

<sup>4</sup>Above 1.5 GeV, electron and muon identification efficiencies are very comparable, so even the statistical features of the two sub-samples are 0similar.

systematics in all cases.

We combine the detector simulation and neutrino reconstruction systematics for a total “experimental systematic,” and then combine this figure in quadrature with the  $b \rightarrow u$  and  $b \rightarrow c$  modeling systematics to arrive at a total systematic error. Combining this in quadrature with the statistical error, we compute a total error which is used in setting limits on the impact ratio correction factors, which we discuss in the next chapter.

**Table 7.2:** Central values and systematic errors for impact ratio  $R_{\text{Endpt}}$ . The column labeled “Expt” includes all neutrino reconstruction systematics (detector,  $K_L$ , secondary leptons), combined in quadrature. The  $b \rightarrow u$  and  $b \rightarrow c$  modeling systematics are evaluated as described in the text. The quadrature combination of all three kinds of systematics errors is shown in the “Syst” heading, which is then combined with the statistical error in quadrature to obtain the entry in the “Total” column. Consult Table 6.1 for a mapping from sample name to other characteristics of the WA samples, such as  $\langle M_X \rangle$  or  $\langle E_\ell \rangle$ .

Sample	$R_{\text{Endpt}}$	Stat	Expt	$b \rightarrow c$	$b \rightarrow u$	Syst	Total
WA01	0.0614	0.0339	0.0162	0.0101	0.0052	0.0198	0.0393
WA02	0.0356	0.0347	0.0148	0.0083	0.0050	0.0177	0.0389
WA03	0.0208	0.0376	0.0147	0.0071	0.0050	0.0170	0.0412
WA04	0.0190	0.0401	0.0157	0.0072	0.0057	0.0182	0.0441
WA05	0.0295	0.0447	0.0196	0.0086	0.0079	0.0229	0.0503
WA06	0.0477	0.0363	0.0176	0.0097	0.0055	0.0208	0.0419
WA07	0.0248	0.0362	0.0143	0.0074	0.0050	0.0168	0.0399
WA08	0.0163	0.0396	0.0174	0.0064	0.0049	0.0192	0.0440
WA09	0.0203	0.0419	0.0178	0.0071	0.0062	0.0201	0.0465
WA10	0.0373	0.0483	0.0220	0.0096	0.0097	0.0259	0.0548
WA11	0.0300	0.0368	0.0147	0.0081	0.0053	0.0176	0.0408
WA12	0.0179	0.0376	0.0167	0.0065	0.0050	0.0186	0.0420
WA13	0.0164	0.0412	0.0168	0.0066	0.0055	0.0188	0.0453
WA14	0.0215	0.0441	0.0191	0.0076	0.0066	0.0216	0.0491
WA15	0.0450	0.0472	0.0217	0.0103	0.0107	0.0263	0.0540
WA16	0.0338	0.0421	0.0175	0.0094	0.0070	0.0211	0.0471
WA17	0.0281	0.0442	0.0189	0.0086	0.0074	0.0221	0.0494
WA18	0.0308	0.0442	0.0196	0.0089	0.0080	0.0230	0.0498
WA19	0.0456	0.0467	0.0247	0.0114	0.0103	0.0291	0.0550
WA20	0.0639	0.0537	0.0243	0.0150	0.0143	0.0320	0.0625
WA21	0.0391	0.0456	0.0224	0.0108	0.0086	0.0263	0.0527
WA22	0.0392	0.0463	0.0179	0.0116	0.0097	0.0234	0.0519
WA23	0.0437	0.0477	0.0177	0.0120	0.0109	0.0240	0.0534
WA24	0.0653	0.0508	0.0196	0.0160	0.0139	0.0288	0.0584
WA25	0.0754	0.0554	0.0138	0.0195	0.0161	0.0288	0.0625
WA26	0.0481	0.0520	0.0205	0.0180	0.0142	0.0308	0.0604
WA27	0.0529	0.0542	0.0180	0.0188	0.0146	0.0298	0.0619
WA28	0.0797	0.0578	0.0213	0.0262	0.0167	0.0376	0.0689
WA29	0.0767	0.0579	0.0166	0.0281	0.0182	0.0374	0.0689
WA30	0.0906	0.0596	0.0107	0.0335	0.0204	0.0407	0.0722

**Table 7.3:** Central values and systematic errors for impact ratio  $R_{q^2, M_X}$ . Conventions are the same as in the previous table.

<b>Sample</b>	$R_{q^2, M_X}$	<b>Stat</b>	<b>Expt</b>	$b \rightarrow c$	$b \rightarrow u$	<b>Syst</b>	<b>Total</b>
WA01	0.0286	0.0164	0.0079	0.0049	0.0024	0.0096	0.0190
WA02	0.0166	0.0164	0.0071	0.0040	0.0023	0.0084	0.0185
WA03	0.0099	0.0181	0.0071	0.0035	0.0024	0.0083	0.0199
WA04	0.0097	0.0206	0.0081	0.0038	0.0029	0.0094	0.0227
WA05	0.0175	0.0268	0.0119	0.0052	0.0047	0.0138	0.0301
WA06	0.0222	0.0174	0.0085	0.0047	0.0025	0.0100	0.0200
WA07	0.0116	0.0172	0.0068	0.0035	0.0023	0.0080	0.0190
WA08	0.0080	0.0196	0.0087	0.0032	0.0024	0.0095	0.0218
WA09	0.0108	0.0224	0.0096	0.0038	0.0033	0.0108	0.0249
WA10	0.0231	0.0304	0.0140	0.0061	0.0060	0.0164	0.0346
WA11	0.0142	0.0178	0.0071	0.0039	0.0025	0.0085	0.0197
WA12	0.0087	0.0186	0.0083	0.0032	0.0024	0.0092	0.0208
WA13	0.0085	0.0216	0.0089	0.0035	0.0028	0.0099	0.0237
WA14	0.0121	0.0250	0.0109	0.0044	0.0037	0.0123	0.0279
WA15	0.0301	0.0321	0.0148	0.0071	0.0071	0.0179	0.0367
WA16	0.0183	0.0231	0.0097	0.0052	0.0038	0.0116	0.0258
WA17	0.0158	0.0252	0.0109	0.0050	0.0041	0.0126	0.0282
WA18	0.0188	0.0273	0.0122	0.0055	0.0049	0.0142	0.0308
WA19	0.0304	0.0317	0.0169	0.0078	0.0068	0.0198	0.0374
WA20	0.0504	0.0430	0.0196	0.0121	0.0112	0.0256	0.0500
WA21	0.0250	0.0296	0.0146	0.0071	0.0055	0.0171	0.0342
WA22	0.0262	0.0313	0.0122	0.0079	0.0064	0.0159	0.0351
WA23	0.0312	0.0345	0.0129	0.0087	0.0077	0.0174	0.0386
WA24	0.0512	0.0405	0.0156	0.0128	0.0108	0.0229	0.0465
WA25	0.0685	0.0508	0.0126	0.0179	0.0144	0.0262	0.0572
WA26	0.0398	0.0435	0.0172	0.0151	0.0117	0.0257	0.0505
WA27	0.0453	0.0468	0.0156	0.0163	0.0124	0.0257	0.0534
WA28	0.0723	0.0528	0.0195	0.0241	0.0149	0.0344	0.0630
WA29	0.0743	0.0562	0.0161	0.0273	0.0173	0.0361	0.0668
WA30	0.0974	0.0636	0.0114	0.0356	0.0214	0.0431	0.0768

**Table 7.4:** Central values and systematic errors for impact ratio  $R_{M_X}$ . Conventions are the same as in the previous table.

<b>Sample</b>	$R_{M_X}$	<b>Stat</b>	<b>Expt</b>	$b \rightarrow c$	$b \rightarrow u$	<b>Syst</b>	<b>Total</b>
WA01	0.0164	0.0095	0.0046	0.0029	0.0014	0.0056	0.0110
WA02	0.0095	0.0094	0.0041	0.0023	0.0013	0.0048	0.0106
WA03	0.0057	0.0104	0.0041	0.0020	0.0013	0.0047	0.0114
WA04	0.0055	0.0118	0.0047	0.0022	0.0016	0.0054	0.0130
WA05	0.0100	0.0154	0.0069	0.0030	0.0027	0.0080	0.0174
WA06	0.0127	0.0100	0.0049	0.0027	0.0014	0.0058	0.0116
WA07	0.0066	0.0099	0.0039	0.0020	0.0013	0.0046	0.0109
WA08	0.0045	0.0112	0.0050	0.0018	0.0013	0.0054	0.0124
WA09	0.0061	0.0128	0.0055	0.0022	0.0019	0.0062	0.0142
WA10	0.0132	0.0176	0.0081	0.0036	0.0035	0.0095	0.0200
WA11	0.0081	0.0102	0.0041	0.0023	0.0014	0.0049	0.0113
WA12	0.0050	0.0106	0.0048	0.0019	0.0014	0.0053	0.0119
WA13	0.0049	0.0123	0.0051	0.0020	0.0016	0.0057	0.0136
WA14	0.0069	0.0143	0.0063	0.0025	0.0021	0.0071	0.0160
WA15	0.0173	0.0187	0.0087	0.0042	0.0041	0.0105	0.0214
WA16	0.0104	0.0133	0.0056	0.0030	0.0021	0.0067	0.0149
WA17	0.0090	0.0145	0.0063	0.0029	0.0024	0.0073	0.0162
WA18	0.0107	0.0157	0.0070	0.0032	0.0028	0.0082	0.0177
WA19	0.0175	0.0184	0.0099	0.0046	0.0039	0.0116	0.0218
WA20	0.0292	0.0254	0.0117	0.0072	0.0066	0.0152	0.0296
WA21	0.0143	0.0171	0.0085	0.0041	0.0031	0.0099	0.0197
WA22	0.0150	0.0181	0.0071	0.0046	0.0037	0.0092	0.0203
WA23	0.0179	0.0200	0.0075	0.0051	0.0045	0.0101	0.0224
WA24	0.0296	0.0239	0.0093	0.0077	0.0063	0.0136	0.0275
WA25	0.0400	0.0305	0.0076	0.0109	0.0086	0.0159	0.0344
WA26	0.0230	0.0255	0.0102	0.0090	0.0068	0.0152	0.0297
WA27	0.0263	0.0277	0.0093	0.0098	0.0073	0.0153	0.0317
WA28	0.0426	0.0322	0.0120	0.0149	0.0090	0.0211	0.0385
WA29	0.0438	0.0342	0.0099	0.0169	0.0104	0.0222	0.0408
WA30	0.0582	0.0396	0.0071	0.0226	0.0131	0.0271	0.0480

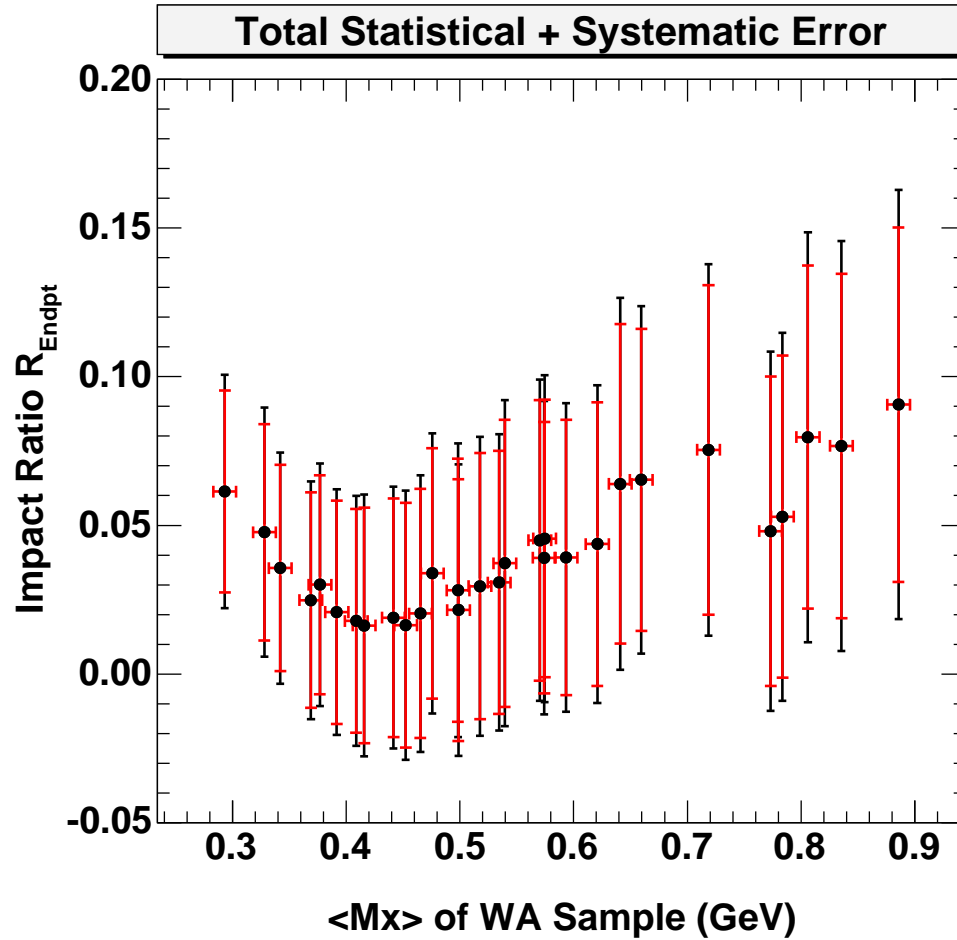


**Figure 7.6:** Parametric plot of endpoint analysis impact ratios, with all uncertainties. The inner set of error bars are statistical; the outer ones include detector and neutrino reconstruction systematics combined in quadrature with  $b \rightarrow u$  and  $b \rightarrow c$  model dependence estimates.

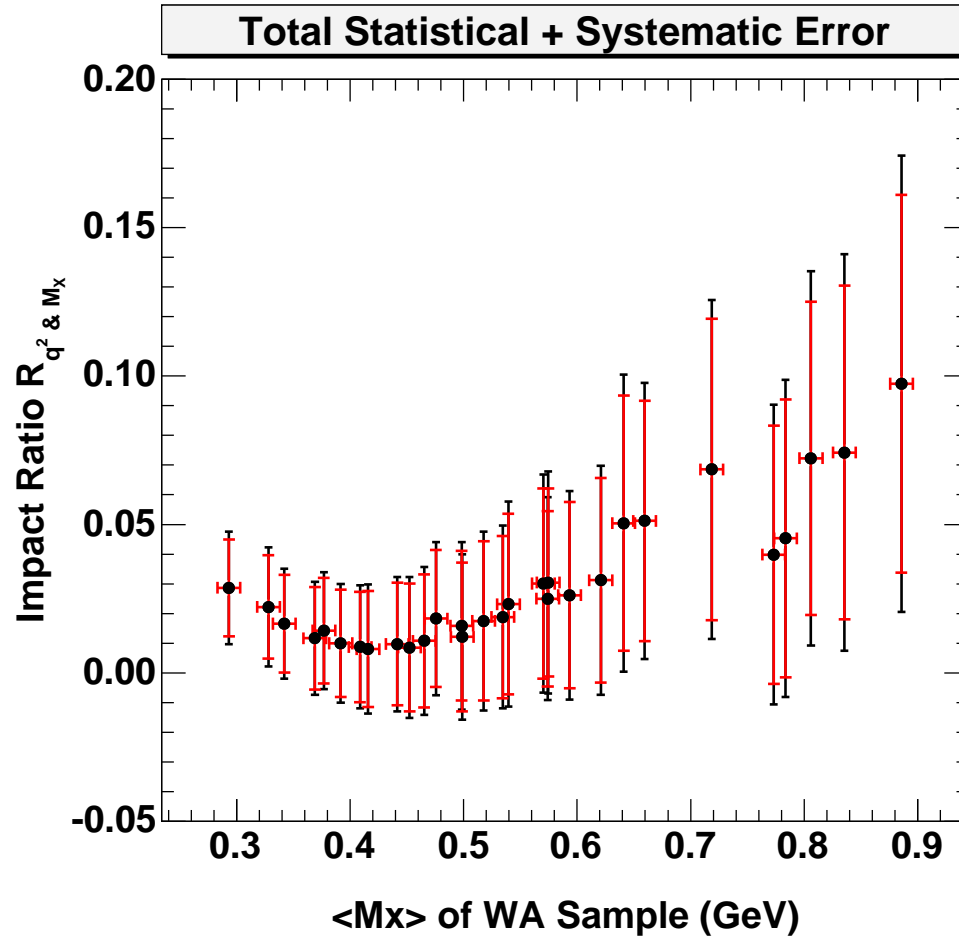


**Figure 7.7:** Parametric plot of  $(q^2, M_X)$  analysis impact ratios, with all uncertainties. The inner set of error bars are statistical; the outer ones include detector and neutrino reconstruction systematics combined in quadrature with  $b \rightarrow u$  and  $b \rightarrow c$  model dependence estimates.

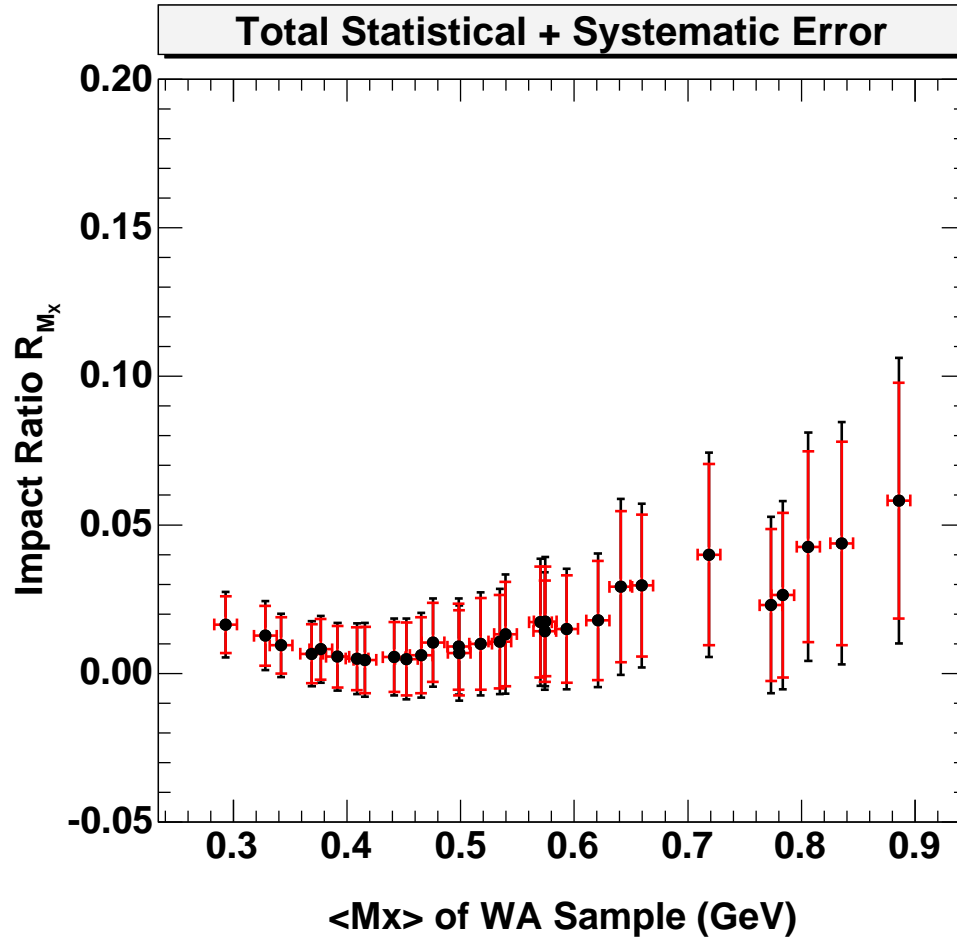


**Figure 7.8:** Parametric plot of  $(M_X)$  analysis impact ratios, with all uncertainties. The inner set of error bars are statistical; the outer ones include detector and neutrino reconstruction systematics combined in quadrature with  $b \rightarrow u$  and  $b \rightarrow c$  model dependence estimates.